Clays and Clay Minerals, Vol. 57, No. 1, 82–92, 2009.

BROMIDE-ION DISTRIBUTION IN THE INTERLAYER OF THE LAYERED DOUBLE HYDROXIDES OF Zn AND Al: OBSERVATION OF POSITIONAL DISORDER

S. V. PRASANNA[1], A. V. RADHA[1], P. V. KAMATH[1,*], AND S. KANNAN[2]

[1] Department of Chemistry, Central College, Bangalore University, Bangalore 560 001, India
[2] Discipline of Inorganic Materials and Catalysis, Central Salt and Marine Research Institute (Council of Scientific and Industrial Research), G.B. Marg, Bhavnagar 364 002, India

Abstract—Because of the anisotropy in bonding, layered hydroxides crystallize with extensive structural disorder due to the incorporation of stacking faults. In contrast, the loss of crystallinity in Br^--ion intercalated layered double hydroxides (LDHs) arises due to the positional disorder of Br^- in the interlayer. The structure of the interlayer in other LDHs is poorly understood due to the low X-ray scattering power of the commonly found anions such as Cl^- and NO_3^- relative to that of the metal hydroxide layers. On heating to 175ºC, the Br^- ion migrates from positions of lesser site degeneracy to those of greater site degeneracy as dehydration of the interlayer opens up access to positions hitherto occupied by intercalated water molecules. The new (18*h*) site is situated closer to the proton of the metal hydroxide layer (1.809 Å) compared to the 6*c* site (2.402 Å). This shows a pre-association of the bromide ion with the proton of the hydroxide layer leading to the release of HBr upon decomposition of the bromide-containing LDHs. The fact that Cl^--containing LDHs also decompose with the evolution of HCl shows that such a redistribution of the atoms in the interlayer is more common than is generally recognized.

Key Words—Layered Double Hydroxides, Positional Disorder, Thermal Studies.

INTRODUCTION

Layered double hydroxides are a class of inorganic layered materials with applications in catalysis (Sels *et al.*, 2001), water purification (Prasanna *et al.*, 2006, 2007), carbon-dioxide fixation (Reddy *et al.*, 2006), and drug-delivery systems (Del Hoyo, 2007). The utility of the LDHs in these applications arises principally from their exchangeable interlayer atoms. The LDHs comprise a stacking of positively charged layers having the composition $[M^{II}_{1-x}M'^{III}_x(OH)_2]^{x+}$ where M = Mg, Ca, Co, Ni, Cu, Zn, and M' = Al, Cr, Fe ($0.2 \leqslant x \leqslant 0.33$) (Cavani *et al.*, 1991). Anions (A^{n-}) and water molecules are intercalated between the metal hydroxide layers. The most common anion in naturally occurring LDHs is CO_3^{2-}. Laboratory-prepared LDHs with other common inorganic ions such as X^- (X = F, Cl, Br, I), NO_3^-, SO_4^{2-}, and others have been reported (de Roy *et al.*, 2001). The LDHs are referred to as $[M-M'-A]_x$.

The stability of the LDHs depends on two factors: (1) the coulombic interactions between the metal hydroxide layers and the intercalated anions, and (2) hydrogen-bonding interactions between the anions and the hydrogen of the hydroxyl groups of the metal hydroxide layer.

The Coulombic interactions are non-directional and depend solely on the magnitude of the charge on the metal hydroxide layers and the anions. On the other hand, hydrogen bonding is highly directional and depends upon a suitable matching of the anion symmetry with the symmetry of the interlayer sites. In the case of monoatomic anions such as X^-, H-bonding is solely determined by its proximity to the hydroxyl ion of the metal hydroxide layer. Thus, in [Zn-Al-X] LDHs, (X = F^-, Cl^-; space group $R\bar{3}m$), the 3*b* site is proximal to the OH^- of the metal hydroxide layer and provides the best opportunity of H-bonding. However, mutual repulsion between the anions of the interlayer causes the X^- ion to move to the 18*h* (or 18*g*) site. This migration to a position of greater site degeneracy introduces a greater degree of disorder, while at the same time compromising on the strength of H-bonding. In contrast, the metal hydroxide layer itself is held together by strong cohesive forces which are iono-covalent in nature.

This anisotropy in bonding introduces extensive structural disorder to the LDHs. The disorders are primarily of two kinds: (1) stacking disorders arising due to the translation or rotation of successive metal hydroxide layers relative to one another; and (2) positional disorder of atoms in the interlayer.

Earlier work on the structural disorder among LDHs focused exclusively on various models of stacking disorders (Radha *et al.*, 2005, 2007; Thomas *et al.*, 2004). The disorder in the interlayer was ignored, at least in part, because the commonly found anions such as CO_3^{2-}, NO_3^-, and Cl^- are poor scatterers compared to the metal hydroxide layers. An extreme manifestation of this approach is seen in the work of Bookin and Drits (1993), who, in their calculations of the structure factors, ignored the interlayer altogether.

The poor attention paid to the structure of the interlayer has a phenomenological basis:

* E-mail address of corresponding author:
vishnukamath8@hotmail.com
DOI: 10.1346/CCMN.2009.0570108

(1) The interlayer is disordered and so it contributes only to diffuse scattering, much like that of the liquid phase.

(2) The anions in the interlayer have high diffusion coefficients (Oesten and Böhm, 1993) which again is manifested as disorder.

(3) In addition to this dynamic disorder, the anions occupy positions of great site degeneracy.

(4) Positional disorder is also possible, arising when the intercalated atoms occupy more than one site in the interlayer.

Molecular modeling and computer simulations are unable to resolve these difficulties as they overemphasize coulombic interactions and underplay the role of weak interactions, which actually determine the anion positions. Furthermore, most numerical calculations assume a cation-ordered lattice, while in actual fact many LDHs are cation disordered (Bellotto *et al.*, 1996).

In light of these factors, the structure of the interlayer has not been studied adequately. The most significant work in this area was done by Ennadi *et al.* (2000), who, by means of the Rietveld method, examined various structure models based on the location of the Cl^- ion in different interlayer sites of the $[Zn\text{-}Al\text{-}Cl]_{0.33}$ LDH.

Using a combination of *DIFFaX* simulations and Rietveld refinement, the structure of the interlayer in the $[Zn\text{-}Al\text{-}Br]_{0.33}$ LDH was examined here. The Br^- ion, being a strong scatterer gives signature reflections in the X-ray powder diffraction (XRD) pattern of the LDH, when it is located in different sites.

EXPERIMENTAL

Preparation of LDHs

$[Zn\text{-}Al\text{-}Cl]_{0.33}$ and $[Zn\text{-}Al\text{-}Br]_{0.33}$ LDHs were prepared by coprecipitation. In a typical preparation, 50 mL of the mixed-metal ($M^{2+} + M^{3+}$) halide salt solution in 2:1 mole ratio was added to a solution (100 mL) containing ten times the stoichiometric requirement of the halide ion taken as its Na^+/K^+ salt. A constant pH = 8 was maintained during precipitation, by the simultaneous addition of 2 N NaOH using a Metrohm Model 718 STAT titrino operating in the pH stat mode. All precipitations were carried out at constant temperature (65ºC); N_2 gas was bubbled through the solution continuously. In each case, the slurry obtained was aged at 65ºC for 18 h under N_2 and then filtered rapidly under suction. The precipitate was washed with warm decarbonated water several times and finally with acetone before being dried at 65ºC.

Wet chemical analysis was carried out to determine the Br^- and Cl^- ion contents of the LDHs. A preweighed (0.2 g) quantity of the sample was dissolved in acid (2 mL of conc. HNO_3) and titrated against standard silver nitrate (0.025 N) solution potentiometrically. The halide content was found to be consistent with the nominal composition ([Zn-Al-Br]: Obs. 32 mol%; Exp. 33 mole%, [Zn-Al-Cl]: Obs. 31 mol%; Exp. 33 mole %).

Characterization

All the samples were characterized by X-ray powder diffraction (XRD) using a Philips X'pert X-ray diffractometer (X'Celerator detector) operated in reflection geometry. Data were collected with CuKα radiation (λ = 1.541 Å) using a step size of 0.017º2θ. The total collection time was 120 min over the range 5−70º2θ.

In situ variable-temperature XRD was carried out on a Philips X'pert MPD system connected to an Anton-Paar high-temperature XRK assembly using CuKα radiation. The sample was mounted in a high-temperature cell and heated at 5ºC min^{-1} in steps of 25ºC and stabilized for 10 min before measurements. The operating voltage and current were 40 kV and 40 mA, respectively. The step size was 0.03º2θ with step time of 1 s.

The samples were also characterized by thermogravimetric analysis (TGA) (Mettler Toledo TGA/SDTA 851^e, Star^e 7.01). The samples were dried to constant weight at 100ºC in the TG balance to expel adsorbed water before the temperature was ramped (100−800ºC, heating rate 5ºC min^{-1}, flowing air).

Computational studies

Rietveld refinements were carried out using the *FULLPROF.2k* code (Version 3.3 June 2005-LLB JRC) (Rodriguez-Carvajal, 2000). In the refinement of the $[Zn\text{-}Al\text{-}Cl]_{0.33}$ structure, a modified pseudo-Voigt lineshape function with five variables (*U*, *V*, *W*, *X*, and η) was employed. To refine the $[Zn\text{-}Al\text{-}Br]_{0.33}$ structure, the Pearson VII correction was also used to fit the experimental profile. The background was refined using a six-coefficient polynomial function.

The XRD patterns were simulated using the FORTRAN-based computer program *DIFFaX*, the formalism of which treats a solid as a stacking of layers of atoms (Treacy *et al.*, 1991). In the present instance, each layer comprises a metal hydroxide layer and an interlayer. The interlayer has the composition $[X^-\cdot H_2O]$ (X = Cl^-, Br^-). The position coordinates of the atoms within the metal hydroxide layer were defined according to the published structure of $[Zn\text{-}Al\text{-}Cl]_{0.33}$ LDH (International Crystal Structure Database No. CC 91155, space group $R\bar{3}m$, a = 3.084(2) Å, c = 23.470(6) Å). The O atom of the intercalated water molecule and the Cl^- ions share a single set of sites (18*h*; 0.129(2), −0.129(2), 0.5). The XRD patterns of model structures were simulated by placing the X^- ion in other sites in the interlayer. Within the $R\bar{3}m$ space group a number of sites can potentially accommodate the X^- ion. Table 1 gives the various sites and their coordinates. Of these, the 18*g* site was not considered because it is in close proximity to the 18*h* site and the two cannot be distinguished by powder diffraction. Model structures were generated by placing the X^- ions in other interlayer sites 3*b* and 6*c*. Positional disorder was generated by distributing the X^-

Table 1. R_{wp} values measuring the goodness of fit of the observed XRD pattern with the *DIFFaX* simulated patterns for different model structures with Br^- ions in different Wyckoff's positions.

Wyckoff's position	*x*	*y*	*z*	R_{wp}	
				$[Zn\text{-}Al\text{-}Br]_{0.33}$	$[Zn\text{-}Al\text{-}Cl]_{0.33}$
18*g*	0.1524	0	0.5	–	–
18*h*	0.1524	−0.1524	0.5	0.205	0.209
3*b*	0	0	0.5	0.385	0.222
6*c*	0	0	0.1667	0.214	0.225
(18*h*, 3*b*)	–	–	–	0.259	0.173
(3*b*, 6*c*)	–	–	–	0.285	0.180
(18*h*, 6*c*)	–	–	–	0.162	0.183

ion in more than one site. In all these models, the position of the O atom of intercalated water was held invariant at the 18*h* site. The position coordinates of all the symmetry-related atoms were specified explicitly and the point group declared as unknown. The *DIFFaX* code then computes the Laue symmetry.

The layers were stacked one on top of another using the stacking vector (2/3, 1/3, 1/3). Such stacking corresponds to the $3R_1$ polytype. The Laue symmetry was computed to be $\bar{3}m$, which is compatible with the $R\bar{3}m$ space group. For model simulations, the cell parameters of the published structures were used. For simulations of experimental patterns, the cell parameters were estimated as $a = 2 \times d_{110}$ and $c = 6 \times d_{006}$.

For model simulations, the calculated Bragg reflections were broadened using a Lorentzian shape (FWHM = 0.2°2θ). For simulations of experimental patterns, a pseudo-Voigt line shape was employed. The best fit of the experimental profile with the simulated pattern was realized by matching the peak position (within ±0.2°2θ), FWHM value (within ±0.1°2θ), and relative intensity (within ±5%) of the 015 reflection. This generally did not result in a good match of the other reflections. Only when the Br^- ions were located in the 18*h* and 6*c* sites was a good match of all the reflections observed.

A nominal 5% stacking disorder was incorporated to make subtle improvements. In LDHs, stacking disorder generally refers to the intergrowth of two polytypes. The $2H_1$ polytype is generated by defining two layers AC and CA and then stacking them one on top of the other using the stacking vector (0, 0, ½). The simultaneous use of more than one stacking vector with different probabilities results in a crystal with stacking disorders.

Turbostraticity is an extreme type of stacking disorder. A stacking vector incorporating a random translation (*x*, *y*, 1) (*x*, *y*: random) introduces turbostratic disorder by destroying the registry between the layers.

The goodness of fit was quantified by evaluating the R_{wp} values (Table 1). The profile parameters and the atom position coordinates used for the simulation of the XRD pattern of the [Zn-Al-Br] LDH are given in Table 2.

Table 2. Input parameters used for the *DIFFaX* simulation of the $[Zn\text{-}Al\text{-}Br]_{0.33}$ LDH.

Atom	Wyckoff's position	*x*	*y*	*z*	SOF
Zn	3*a*	0.0000	0.0000	0.0000	0.6667
Al	3*a*	0.0000	0.0000	0.0000	0.3333
O1	6*c*	0.0000	0.0000	0.3765	1.0000
O2	18*h*	0.1524	−0.1524	0.5000	0.0666
Br1	18*h*	0.1524	−0.1524	0.5000	0.0275
Br2	6*c*	0.0000	0.0000	0.1667	0.0825
		Shape parameters			
Laue symmetry		*U*	*V*	*W*	η
$\bar{3}m$		0.6200	−0.0230	0.052	0.1063
Cell parameters					
a (Å)	3.081				
c (Å)	23.723				
Stacking vector	(2/3, 1/3, 1/3)				
Stacking disorder	8%				
R_{wp}	0.162				

SOF: site occupancy factor

More details of the *DIFFaX* simulations of the LDHs can be found in previous works (Radha *et al.*, 2005, 2007; Thomas *et al.*, 2004). A typical *DIFFaX* input file used for the simulation of the XRD pattern of the [Zn-Al-Br] LDH is given in the Supporting Information document SI.1, available from The Clay Minerals Society's online depository at www.clays.org/journal/JournalDeposits.html.

RESULTS AND DISCUSSION

Within the LDH structure, the interlayer atoms can potentially occupy the 3*b*, 6*c*, or the 18*h* sites (Figure 1). Of these, the 3*b* site is equidistant between the hydroxyl groups of the adjacent layers, while the 18*h* site corresponds to a set of six different sites located at the vertices of a hexagon, centered around the 3*b* site. The 6*c* position is just below the metal ions and corresponds to the prismatic interlayer site.

The *DIFFaX*-simulated XRD patterns of model structures obtained by placing the Cl^- ion in the three different interlayer positions (Figure 2) do not differ greatly from one another. Incorporation of positional disorder, corresponding to the location of Cl^- ions in more than one site makes the calculated patterns practically indistinguishable from one another (Supporting Information SI.2, available from The Clay Minerals Society's online depository at http://www.clays.org/journal/JournalDeposits.html). The insensitivity of the XRD pattern to the structure of the interlayer is due to the poor scattering power of the interlayer atoms relative to the metal hydroxide layers.

When a strong scatterer such as Br^- is included in the interlayer, the situation is different (Figure 3). A dramatic increase is observed in the intensity of the 006 reflection relative to 003 on account of the greater electron density in the interlayer. The contribution of the metal hydroxide sublattice to the diffraction intensity has been compared with that made by the interlayer atoms (Thomas *et al.*, 2004). The interlayer atoms diffract out of phase with the metal hydroxide sublattice, by virtue of which, the 006 reflection is enhanced in intensity relative to the 003 reflection.

In the mid-2θ (30−55º2θ) region, the intensity of the 015 reflection correlated directly with the location of the Br^- ion in the 6*c* site. In the high-angle region (>50º2θ), the relative intensities of the 110 and 113 reflections remained unchanged when the Br^- was located in 3*b* and 6*c* sites, while the intensity of the 113 reflection increased relative to the 110 reflection when the 18*h* sites were occupied.

As the 015 reflection is least affected by stacking disorder (Thomas and Kamath, 2006), matching this reflection required the incorporation of positional disorder. The effect of positional disorder of the Br^- ions in the interlayer on the XRD patterns (Supporting Information SI.3 available from The Clay Minerals Society's online depository at www.clays.org/journal/JournalDeposits.html) showed that the distribution of the Br^- ions in the (18*h*, 3*b*) sites is distinguishable from

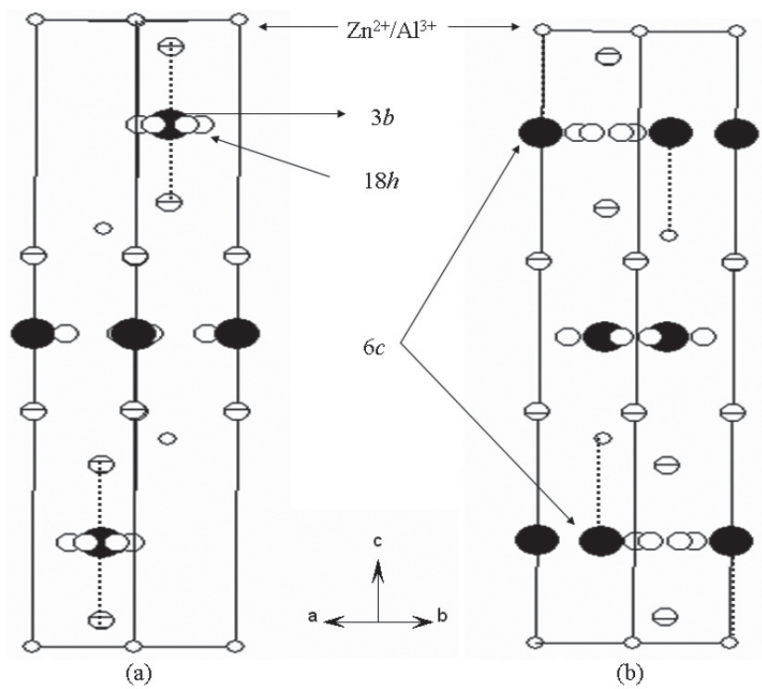

Figure 1. Schematic representation of (a) 3*b* and 18*h*, and (b) 6*c* sites in the interlayer. Hatched circles correspond to the hydroxyl ions of the metal hydroxide layers. The dotted lines show the proximity of the interlayer sites to the atoms in the layer.

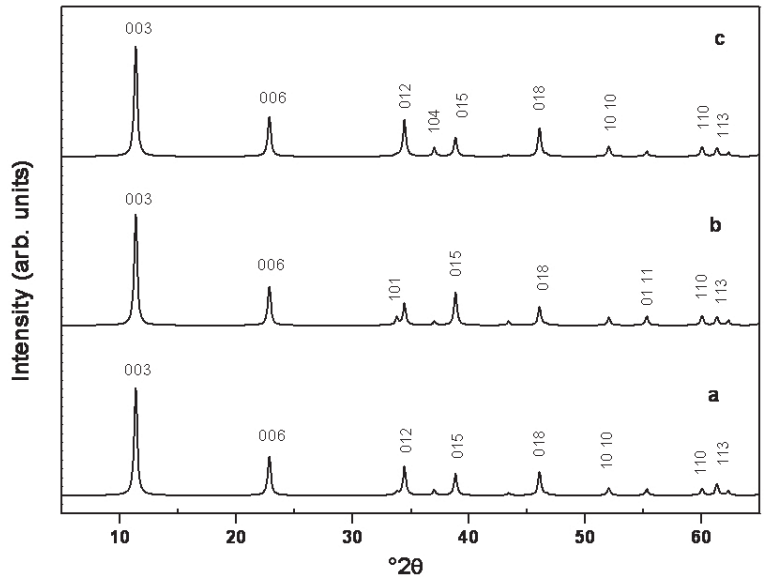

Figure 2. *DIFFaX*-simulated XRD patterns of the [Zn-Al-Cl]$_{0.33}$ LDH with Cl^- in (a) 18*h*, (b) 6*c*, and (c) 3*b* positions.

that in the (18*h*, 6*c*) sites. The 6*c* site has hitherto not been proposed in any of the published structure models.

The XRD patterns of the pristine [Zn-Al-*X*]$_{0.33}$ (*X* = Cl^-, Br^-) LDHs (Figure 4) revealed that the peaks corresponding to the different reflections were uniformly broadened and the patterns are, in general, representative of phases without significant stacking disorders. The published structure models favor the 18*h* site as that probably occupied by the interlayer halide ion (Ennadi *et al.*, 2000; Roussel *et al.*, 2000). Therefore, the observed XRD pattern of the [Zn-Al-Br]$_{0.33}$ LDH was compared with the *DIFFaX*-simulated pattern of the model structure containing Br^- ions in the 18*h* site (Figure 5a). While the peak positions matched, the discrepancies in the relative intensities of the 0*kl* reflections are obvious. Discrepancies were attributed (by Bellotto *et al.*, 1996) to the presence of stacking disorders. The best match was obtained by adopting the stacking disorder model incorporating 20% of $2H_1$ polytype motifs in the matrix of the $3R_1$ polytype (Figure 5b). While the stacking disorder model was very successful at explaining the variation in the line shapes

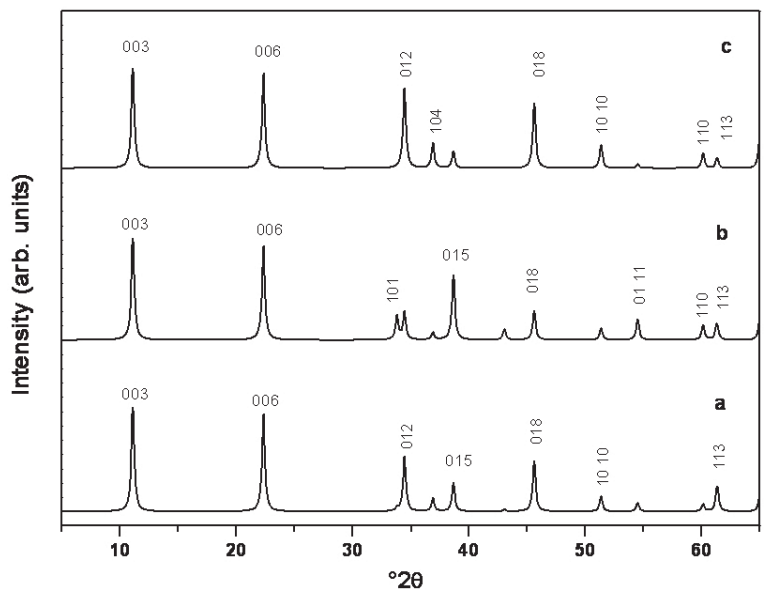

Figure 3. *DIFFaX*-simulated XRD patterns of the [Zn-Al-Br]$_{0.33}$ LDH with Br^- in (a) 18*h*, (b) 6*c*, and (c) 3*b* positions.

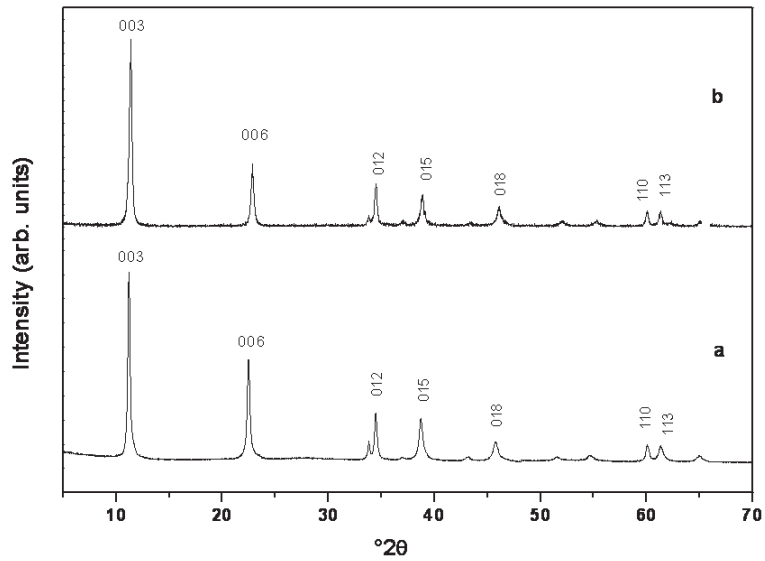

Figure 4. XRD pattern of pristine (a) $[Zn\text{-}Al\text{-}Br]_{0.33}$ and (b) $[Zn\text{-}Al\text{-}Cl]_{0.33}$ LDHs.

of the peaks in the mid-2θ region of the XRD patterns of other LDHs (Radha *et al.*, 2007; Bellotto *et al.*, 1996), in the present case, the fit is unsatisfactory because the intensity fails to account for the 015 reflection. The fit could not be improved by the inclusion of motifs corresponding to any other polytype. On the other hand, a satisfactory match of the observed pattern was found with the pattern simulated by the structure model incorporating positional disorder (18*h*, 6*c*) of the Br^- ions (Figure 6). The R_{wp} values (Table 1) calculated for the best fit of the observed profile (Figure 4a) with the patterns simulated for the various structure models are evidence that the model incorporating Br^- ions in the 18*h* and 6*c* sites yields the most dramatic improvement in the R_{wp} values among all the models considered. The profile parameters and the position coordinates used for the simulation in Figure 6 are given in Table 2. The site occupancy factors (SOF) of 18*h* and 6*c* were varied to obtain the best fit. A similar approach to the observed XRD pattern of [Zn-Al-Cl] LDH does not produce any improvement in the R_{wp} value (Table 1).

The structure model with Br^- distributed between the 18*h* and the 6*c* sites was, therefore, used for the refinement of the $[Zn\text{-}Al\text{-}Br]_{0.33}$ structure by the

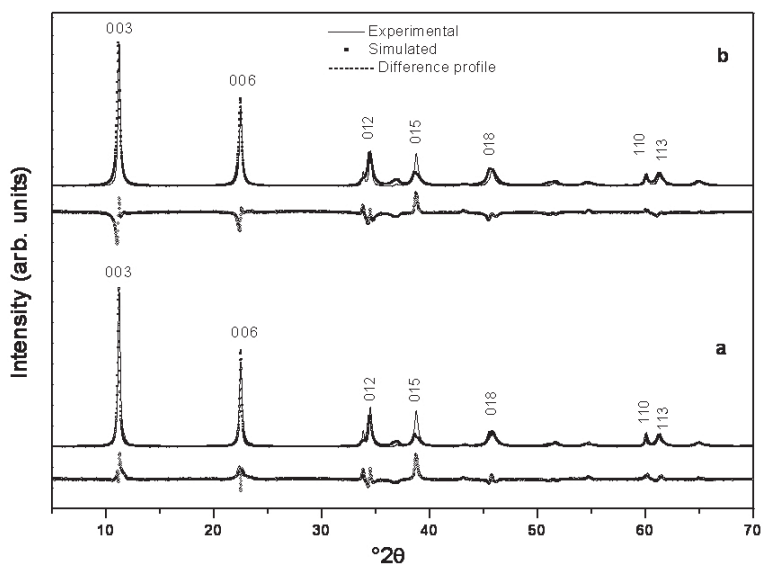

Figure 5. A comparison of the XRD pattern of the $[Zn\text{-}Al\text{-}Br]_{0.33}$ LDH with the *DIFFaX*-simulated pattern (Br^- in the 18*h* site) (a) without and (b) with the incorporation of stacking disorders.

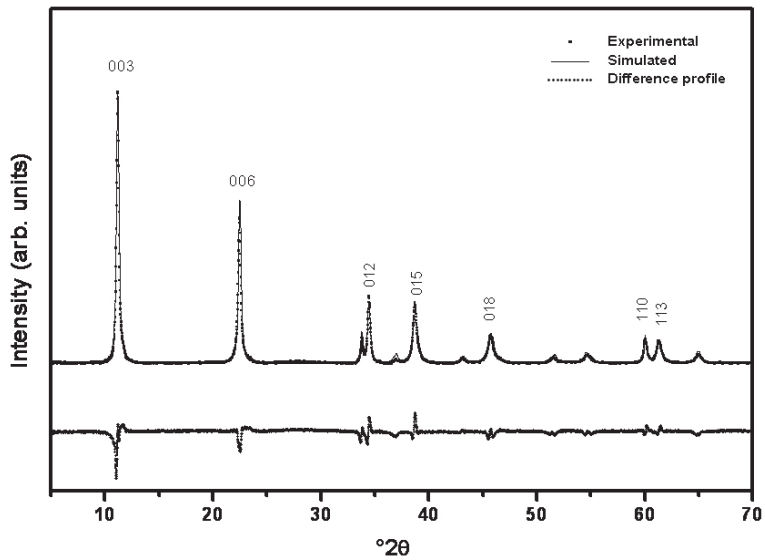

Figure 6. A comparison of the XRD pattern of the $[Zn-Al-Br]_{0.33}$ LDH with the pattern simulated using the positional disorder model (Br^- in the 18*h* and 6*c* sites).

Rietveld method (Figure 7). The various structural parameters and the goodness-of-fit parameters are given in Tables 3 and 4. Refinement was also carried out with the structure model incorporating Br^- exclusively in the 18*h* site (Table 3). The superiority of the structure incorporating positional disorder is obvious.

The results of structure refinement of the $[Zn-Al-Cl]_{0.33}$ LDH (see Table 3) are similar to those reported by Ennadi *et al.* (2000) and are not repeated here. The average bond distances and angles calculated from the refined parameters of various structure models offer a true insight into the environment of the Br^- ion in the interlayer. The O1–O1 distance of shared octahedral edges increases from 2.696 Å when Br^- ions are positioned in 18*h* site to 2.722 Å when the Br^- ions are distributed in 18*h* and 6*c* sites. This reflects a slight elongation of the hydroxyl octahedra. Consequently, the average metal–O1 distance increases when the Br^- ions are positionally disordered. The interactions between the layer oxygen and the interlayer oxygen becomes stronger as shown by the reduced O1–(O2, Br1) distance in the presence of positional disorder. However, the larger O1–Br2 distance of 3.42 Å in comparison with O1–Br1 distance of 3.04 Å indicates that Br^- ions in the 18*h* position have a greater interaction with the metal hydroxide layers than the Br^- ions in 6*c* sites. The 6*c*

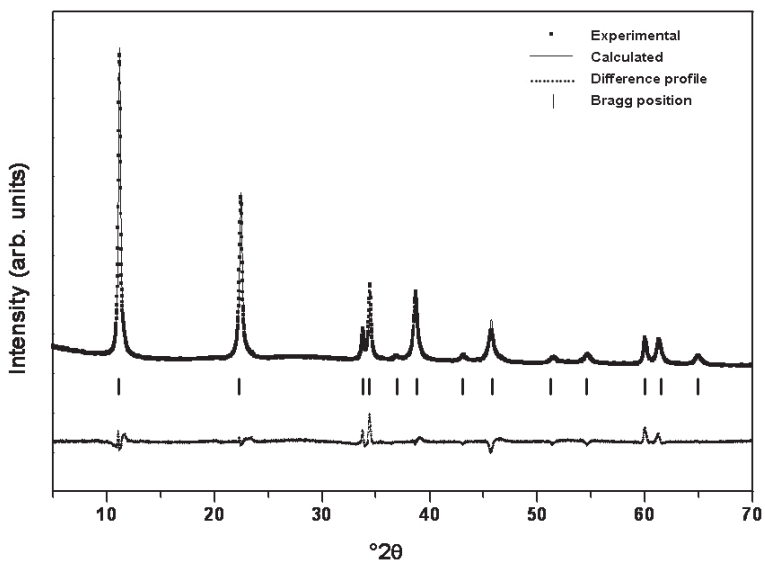

Figure 7. Rietveld refinement of the structure of $[Zn-Al-Br]_{0.33}$ LDH.

Table 3. Results of Rietveld refinements of [Zn-Al-X]$_{0.33}$ (X = Br^- and Cl^-) LDHs.

Space group	Br^- in 18*h* $R\bar{3}m$	Br^- in (18*h*, 6*c*) $R\bar{3}m$	Cl^- in 18*h* $R\bar{3}m$
Cell parameters			
a (Å)	3.0806 (3)	3.0802 (7)	3.0813 (3)
c (Å)	23.7570 (1)	23.7604 (2)	23.351 (5)
Shape parameters			
U	1.2538 (2)	0.6394 (1)	0.0270 (1)
V	−0.0385 (1)	−0.0245 (3)	−0.0316 (2)
W	0.03611(9)	0.0524 (8)	0.0877 (1)
X	0.0073 (1)	0.1063 (1)	0.0016 (2)
Y	–	−0.0078 (1)	–
η (or *m*)	0.9705 (1)	0.7031 (5)	0.4175 (4)
Goodness of fit			
R_{wp}	0.257	0.181	0.396
R_{Bragg}	0.105	0.040	0.097
R_{F}	0.065	0.051	0.865
R_{P}	0.278	0.192	0.031
χ^2	0.153	0.074	0.028
Distances (Å)			
(Zn, Al)−O1	2.046 (15)	2.055 (5)	2.054 (15)
O1− O1	2.696 (11)	2.722 (3)	2.715 (11)
O1−(O2, X1)	3.066 (2)	3.040 (1)	2.986 (2)
(O2, X1)−(O2, X1)	2.668 (3)	2.670 (8)	2.668 (3)
(Zn, Al) − Br2	–	3.967 (7)	–
O1 − Br2	–	3.420 (3)	–
(O2, X1) − Br2	–	1.542 (4)	–
Angles (º)			
O1−(Zn, Al)−O1	97.61 (14)	97.05 (6)	97.12 (6)
	82.39 (11)	82.95 (4)	82.78 (12)

site corresponds to a trigonal prismatic site in the interlayer which is larger than the octahedral sites. Therefore, the 6*c* site is preferred by the larger Br^- ion (ionic radius, 1.96 Å) while the smaller Cl^- ion (ionic radius, 1.81 Å) prefers the adjacent 18*h* site. As a result, the interlayer distance in the [Zn-Al-Br]$_{0.33}$ LDH remains largely unchanged in comparison with the [Zn-Al-Cl]$_{0.33}$ LDH.

In conclusion, [Zn-Al-Br]$_{0.33}$ LDH has a structure with positional disorder with respect to the Br^- ion. The location of a fraction of Br^- ions in the 6*c* site is consistent with the larger size of the 6c site and the absence of H-bonding ability of the Br^- ion. In contrast, the location of the Cl^- ion in the 18*h* site is consistent with the smaller size and better H-bonding ability of the Cl^- ion.

Thermal treatment of the [Zn-Al-Br]$_{0.33}$ LDH

The *in situ* variable temperature (VT) XRD patterns of [Zn-Al-Br]$_{0.33}$ LDH (Supporting Information SI.4, available from The Clay Minerals Society's online depository at http://www.clays.org/journal/JournalDeposits.html) revealed the following changes on heating:

Table 4. Position parameters obtained from Rietveld refinement of [Zn-Al-Br]$_{0.33}$ LDH.

Atom	Wyckoff's position	*x*	*y*	*z*	B_{iso}	SOF
Zn	3*a*	0.0000	0.0000	0.0000	0.7823(1)	0.6667
Al	3*a*	0.0000	0.0000	0.0000	0.7823(1)	0.3333
O1	6*c*	0.0000	0.0000	0.3767(3)	0.0306(5)	1.0000
O2	18*h*	0.1524(9)	−0.1524(9)	0.5000	1.00000	0.06833(6)
Br1	18*h*	0.1524(9)	−0.1524(9)	0.5000	1.00000	0.02723(6)
Br2	6*c*	0.0000	0.0000	0.1667	1.0228(4)	0.07959(8)

SOF: site occupancy factor

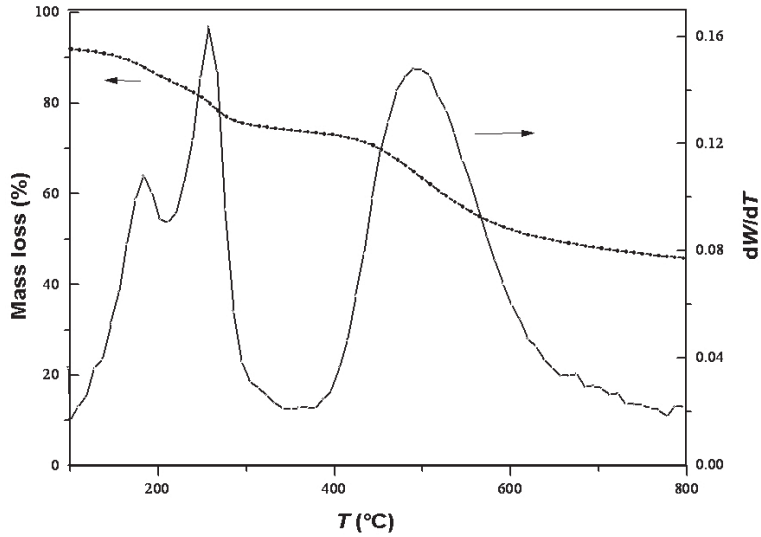

Figure 8. TGA and DTG profile of $[Zn\text{-}Al\text{-}Br]_{0.33}$ LDH.

(1) The intensity of the 003 reflection relative to the 006 reflection increased gradually from 100ºC to 175ºC. These 00*l* and 002*l* reflections also shifted to greater 2θ values, indicating progressive loss of the intercalated water. From the TGA analysis (Figure 8), the mass loss corresponds to 0.38 mole% of H_2O.

(2) With increase in temperature, changes also occurred in the relative intensities of peaks in the mid-2θ region. Up to 150ºC (mass loss 9%), the intensity of the 018 reflection diminished progressively. At 175ºC, the 015 reflection decreased relative to the 012 reflection and the 018 reflection was almost extinguished. At 200ºC, a general broadening was observed of the peaks due to all the reflections.

(3) The decomposition of the LDH was complete by 300ºC. Above this temperature the basal reflections were completely extinguished, indicating the collapse of the layered structure. The observed mass loss of 17.3% at this temperature is in good agreement with the expected mass loss of 18%, which corresponds to the complete dehydration and dehydroxylation of the LDH.

(4) Above 250ºC, features corresponding to ZnO, the crystallinity of which increases with temperature, began to emerge. At 600ºC, peaks attributed to the spinel phase ($ZnAl_2O_4$) can be indexed along with the ZnO phase. An extended mass loss, which was incomplete even at 700ºC, was observed. This can be attributed to the gradual loss of volatile gas (HBr) from the micropores of the oxide residue.

Studies by VT-XRD on Zn-Al LDHs indicate that the LDH decomposes without any change in the stacking sequence of the metal hydroxide layers (Thomas *et al.*, 2006). Therefore, any changes in the mid-2θ and the high-angle reflections in the XRD pattern should be attributed to changes in the interlayer region rather than to changes in the stacking sequence of the metal hydroxide layers. The gradual increase in the intensity of the 015 reflection relative to that of 012 up to 150ºC indicates a change in the environment of the Br^- ion. As explained previously, the intensity of the 015 reflection is related to the occupancy of the 6*c* site relative to that of the 18*h* site (see SI.3). The increase in the intensity of the 015 reflection with increase in temperature signifies the progressive reduction in the occupancy of the 18*h* site through dehydration. The *DIFFaX* simulation of the XRD pattern of the LDH phase at 150ºC (Figure 9a) corresponds to a water content of 0.38 moles per formula unit of the LDH. The site occupancy factor (SOF) of the 18*h* site is reduced from 0.091 in the pristine LDH to 0.049 at 150ºC.

Table 5. Results of *DIFFaX* simulations of $[Zn\text{-}Al\text{-}Br]_{0.33}$ LDH at various temperatures.

Temperature (ºC)	SOF 18*h* O2	SOF 18*h* Br1	SOF 6*c*	SOF 3*b*	Water content (mol %)	% of turbostraticity
Ambient	0.0633	0.0275	0.0825	0.0	0.38	8
150	0.0216	0.0275	0.0825	0.0	0.13	18
175	0.0	0.0296	0.07	0.0	0.0	25
200	0.0	0.33	0.05	0.22	0.0	60

SOF: site occupancy factor

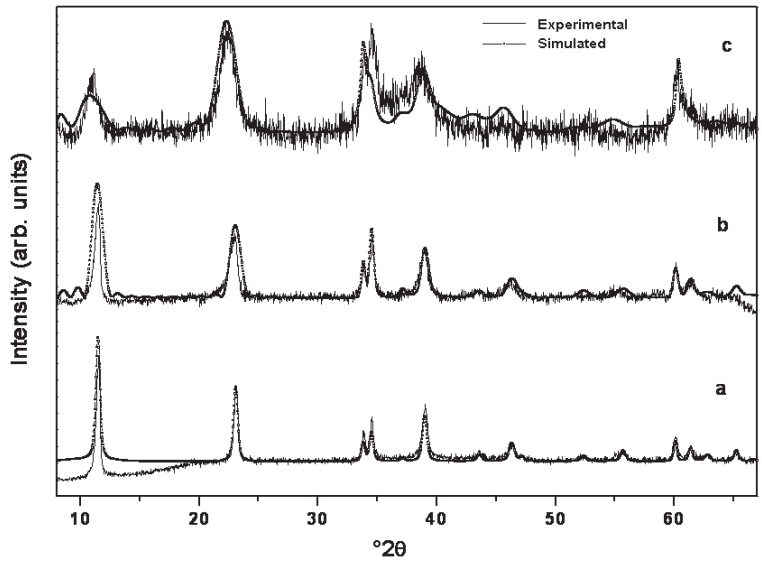

Figure 9. XRD patterns of [Zn-Al-Br]$_{0.33}$ LDH at (a) 150ºC, (b) 175ºC, and (c) 200ºC overlaid with their corresponding *DIFFaX* simulations.

On equilibration at 175ºC, a dramatic change occurred in the mid-2θ region. The inversion in the relative intensities of the 012 and 015 reflections is indicative of a change in the environment of the Br^- ion in the interlayer consequent to dehydration. The excessive broadening of the basal reflections is on account of a decrease in the crystallite size due to mass loss. The corresponding *DIFFaX* simulation (Figure 9b) was achieved by: (1) reducing the occupancy of the Br^- ion in the 6*c* site by 15% and increasing the occupancy in the 18*h* site by the same value; and (2) decreasing the crystallite size to 38 nm corresponding to stacking of 48 layers. This suggests that at 175ºC, the Br^- ion migrates from the 6*c* site to the 18*h* site as dehydration of the interlayer opens up access to positions of greater site degeneracy. The migration of Br^- to the 18*h* site can be related to the mode of decomposition of the [Zn-Al-Br]$_{0.33}$ LDH. The halide-containing LDHs are unique in that they decompose by the release of H*X* rather than X_2 (Kameda *et al.*, 2007). The migration of the Br^- from the 6*c* site to the 18*h* site just before decomposition facilitates the release of HBr, because the Br^- ion in the 18*h* site is situated closer to the proton of the metal hydroxide layer (1.809 Å) compared to the 6*c* site (2.402 Å). This reveals a pre-association of the H and Br atoms prior to the decomposition of the LDH and explains the release of HBr upon the decomposition of the bromide-containing LDHs.

The pre-association is also explicable by hydrogen-bonding considerations. The loss of strongly hydrogen-bonded interlayer water through dehydration leads to a decrease in the hydrogen-bonding interactions with the layer. This necessitates the migration of the Br^- ion to the 18*h* site as the latter is more conducive to weak associations than the 6*c* site. The impetus required for the migration might be provided by the thermal energy and the stabilization incurred upon reduction in the steric factors after dehydration.

The XRD pattern of the LDH phase at 200ºC is indicative of a highly disordered structure. The Zn-Al LDH decomposes to give a defect wurtzite ZnO residue due to strong preference for tetrahedral sites by Zn. The XRD pattern obtained at 200ºC corresponds to the precursor to the wurtzite oxide and could be simulated by incorporating 33% of the total Zn in tetrahedral sites within the interlayer (Figure 9c). The increased electron density of the interlayer produces an inversion in the relative intensities of the basal reflections. The excessive broadening of the reflections was achieved by incorporating crystallite-size effects. The crystallite size obtained from *DIFFaX* is ~4.75 nm and corresponds to the stacking of six layers, indicating the nanoparticulate nature of the oxide residue formed soon after the decomposition of the LDH.

CONCLUSIONS

The XRD data suggest that the Br^- ion in [Zn-Al-Br] LDH is distributed in two crystallographically distinct sites, 18*h* and 6*c*, in the interlayer. In contrast, the poor X-ray scattering power of the interlayer relative to that of the metal hydroxide layers in Cl^--intercalated LDH precludes such a precise description. The changes in the XRD pattern of [Zn-Al-Br] LDH during thermal treatment point to significant variations in the distribution of Br^- ions among the available interlayer sites prior to decomposition of the LDH. The redistribution is consistent with the mode of deanation of Br^- and explains the release of HBr upon thermal decomposition of the LDH.

ACKNOWLEDGMENTS

The authors thank the Department of Science and Technology (DST), Government of India (GOI), for financial support. P.V.K. is a recipient of the Ramanna Fellowship of the DST. S.V.P. thanks the Council of Scientific and Industrial Research (CSIR) for the award of Senior Research Fellowship (SRF).

REFERENCES

Bellotto, M., Rebours, B., Clause, O., Lynch, J., Bazin, D and Elkaim, E. (1996) A reexamination of hydrotalcite crystal chemistry. *Journal of Physical Chemistry*, **100**, 8527–8534.

Bookin, A.S. and Drits, V.A. (1993) Polytype diversity of the hydrotalcite-like minerals 1. Possible polytypes and their diffraction features. *Clays and Clay Minerals*, **41**, 551–557.

Cavani, F., Trifiro, F., and Vaccari, A. (1991) Hydrotalcite-type anionic clays: preparation, properties and applications. *Catalysis Today*, **11**, 173–301.

De Roy, A., Forano, C., and Besse, J.P. (2001) *Layered Double Hydroxides: Past and Future* (V. Rives, editor). Nova Science, New York, pp. 1–37.

Del Hoyo, C. (2007) Layered double hydroxides and human health: An overview. *Applied Clay Science*, **36**, 103–121.

Ennadi, A., Legrouri, A., De Roy, A., and Besse, J.P. (2000) X-ray diffraction pattern simulation for thermally treated [Zn-Al-Cl] layered double hydroxide. *Journal of Solid State Chemistry*, **152**, 568–572.

Kameda, T., Yoshioka, T., Watanabe, K., Uchida, M., and Okuwaki, A. (2007) Dehydrochlorination behavior of a chloride ion-intercalated hydrotalcite-like compound during thermal decomposition. *Applied Clay Science*, **35**, 173–179.

Oesten, R. and Böhm, H. (1993) Ionic mobility in basic double salts. Part 1: Hydrotalcites. *Solid State Ionics*, **62**, 199–204.

Prasanna, S.V., Rao, R.A.P., and Kamath, P.V. (2006) Layered double hydroxides as potential chromate scavengers. *Journal of Colloid and Interface Science*, **304**, 292–299.

Prasanna, S.V., Kamath, P.V., and Shivakumara, C. (2007) Synthesis and characterization of chromate intercalated layered double hydroxides. *Materials Research Bulletin*, **42**, 1028–1309.

Radha, A.V., Shivakumara, C., and Kamath, P.V. (2005) DIFFaX simulations of stacking faults in layered double hydroxides (LDHs). *Clays and Clay Minerals*, **53**, 521–528.

Radha, A.V., Kamath, P.V., and Shivakumara, C. (2007) Conservation of order, disorder and crystallinity during anion exchange reactions among layered double hydroxides (LDHs) of Zn with Al. *Journal of Physical Chemistry B*, **111**, 3411–3418.

Reddy, M.K.R., Xu, Z.P., Lu, G.Q., and da Costa, J.C.D. (2006) Layered double hydroxide for CO_2 capture: Structure evolution and regeneration. *Industrial and Engineering Chemistry Research*, **45**, 7504–7509.

Rodriguez-Carvajal, J. *FullProf2000* Laboratoire Léon Brillouin (UMR12 CEA-NRS): Gif-sur-Yvette Cedex, France, available at www-llb.cea.fr/fullweb/powder.htm (accessed February 2007).

Roussel, H., Briois, V., Elkaïm, E., de Roy, A., and Besse, J.P. (2000) Cationic order and structure of [Zn-Cr-Cl] and [Cu-Cr-Cl] layered double hydroxides: an XRD and EXAFS study. *Journal of Physical Chemistry B*, **104**, 5915–5923.

Sels, B.F., De Vos, D.E., and Jacobs, P.A. (2001) Hydrotalcite-like anionic clays in catalytic organic reactions. *Catalysis Reviews*, **43**, 443–488.

Thomas, G.S. and Kamath, P.V. (2006) Line broadening in the PXRD patterns of layered hydroxides: The relative effects of crystallite size and structural disorder. *Journal of Chemical Science*, **118**, 127–133.

Thomas, G.S., Rajamathi, M., and Kamath, P.V. (2004) DIFFaX simulations of polytypism and disorder in hydrotalcite. *Clays and Clay Minerals*, **52**, 693–699.

Thomas, G.S., Radha, A.V., Vishnu Kamath, P., and Kannan, S. (2006) Thermally induced polytype transformations among the layered double hydroxides (LDHs) of Mg and Zn with Al. *Journal of Physical Chemistry B*, **110**, 12365–12371.

Treacy, M.M.J., Newsam, J.M., and Deem, M.W. (1991) A general recursion method for calculating diffracted intensities from crystals containing planar faults. *Proceedings of Royal Society, London*, **A433**, 499–520.

(*Received 19 May 2008; revised 10 November 2008; Ms. 0160; A.E. T. Kogure*)